

Chapter 4

Gas Hydrate Models



Behzad Partoon, S. Jai Krishna Sahith, Bhajan Lal
and Abdulhalim Shah Bin Maulud

4.1 Introduction

Since the first announcement by Hammerschmidt regarding the blockage of transportation pipelines by gas hydrates, the attempt to overcome the situation was looked into [1]. The first exercises were to utilize the anti-freezing agents, such as methanol or ethylene glycol as additives to prevent the hydrate formation [2]. The presence of these chemicals in the solution was to shift the equilibrium phase boundary conditions of the gas hydrates to much lower temperatures and higher pressure. The addition of methanol to the solution shifted the gas hydrate phase boundary to the left, where gas hydrate formed at much lower temperatures and higher pressure conditions. This behaviour was due to the hydrogen bonding between the water and methanol molecules, which decreased the water activity and the tendency to form hydrate cages [3]. This group of chemicals was referred to as thermodynamic inhibitors. Thermodynamic inhibitors have been widely used in the oil and gas industry for the prevention of gas hydrate formation and blockage in the pipelines and cold processes [4]. On the other hand, some chemicals enhance the hydrate formation by shifting the phase boundary to the right. These additives are thermodynamic promoters. Thermodynamic promoters are normally captured in the hydrate crystalline structure along with the gas molecules. These molecules help to stabilize the hydrate structure at a higher temperature and/or lower pressure. In 1991, Dyadin et al. summarized the hydrate equilibrium temperature of few cyclic esters, such as trimethylene oxide, ethylene oxide, 1,3- and 1,4-dioxane, 1,3-dioxolane, and tetrahydrofuran, at low and high pressures. They claimed that these chemicals, which can form sII under atmospheric pressures, are also able to form hydrates at higher pressures with the help of small gases [5]. These stabilizing chemicals might be effectively used for storing natural gas in solid hydrate state because of their effect on the shift of hydrate forming equilibrium temperature and pressure to milder ones and the large increase in storage capacity. The attempt of predicting the impact of these additives on the gas hydrate phase boundary started with Hammerschmidt in the 1930s. It was very important for the oil and gas industries to predict the proper amount of inhibitors that was required

to eliminate the risks of pipelines' blockage with gas hydrate. The Hammerschmidt formula was based on the suppression of the hydrate formation temperature in the presence of inhibitors, as shown in Eq. (4.1).

$$\Delta T = \frac{k_H W}{M(100 - W)} \quad (4.1)$$

Although the thermodynamic-based approaches were developed in the 1950s, the suppression temperature method is still practiced due to its simplicity and acceptable accuracy. The suppression temperature is the reduction of the equilibrium temperature as a result of additives, and thus, its accuracy is tied in with the accuracy of hydrate equilibrium temperature estimation in the presence of pure samples. On the other hand, the thermodynamic models are mainly based on the equality of chemical potentials of each component in all phases. Hence, any additive to the mixture could also be included in the calculation, if required parameters for prediction of chemical potentials are available. In the following pages, the recent advances on both methods are collected and discussed.

4.2 Classic Thermodynamic Model

The first research for determining the properties of gas hydrate using a statistical thermodynamic approach was done carried out by Barrer and Stuart at 1957 [6]. With the knowledge of the crystal structure of hydrates and using a similar approach, a statistical thermodynamic model of hydrate phase equilibria was conceived by van der Waals and Platteeuw at in 1959 [7]. In their work, expressions for the chemical potential of water in sI and sII hydrate structures were developed using an approach analogous to the Langmuir gas adsorption.

The classic van der Waals and Platteeuw (vdWP) model was based on the difference between the chemical potential of water in the hydrate phase μ_w^H and a hypothetical empty lattice hydrate phase (μ_w^β) as shown in Eq. (4.2).

$$\frac{\Delta\mu_w^H}{RT} = \frac{\mu_w^\beta - \mu_w^H}{RT} = \sum_{m=1}^2 v_m \ln \left(1 + \sum_{i=1}^{nc} C_{mi} f_i \right) \quad (4.2)$$

where v_m is the number of cages of type m in the crystalline structure, C_{mi} is the Langmuir constant of hydrate former i in the type m cage of the crystalline structure, and f_i is the fugacity of hydrate formers.

The vdWP model led Saito et al. [8] and Parrish and Prausnitz [9] to predict the gas hydrate equilibria by equating the chemical potential of water in hydrate, with that in the aqueous (or ice) phase and introducing an algorithm in a form suitable for use on a computer. The expression of the chemical potential of water in an aqueous or ice phase has been simplified by some researchers such as Holder et al. [10] and

John et al. [11] as shown in Eq. (4.3).

$$\frac{\Delta\mu_w^\alpha}{RT} = \frac{\mu_w^\beta - \mu_w^\alpha}{RT} = \frac{\Delta\mu_w^0}{RT} - \int_{T_0}^T \frac{\Delta h_w}{RT^2} dT + \int_{P_0}^P \frac{\Delta v_w}{RT} dP - RT \ln(a_w^\alpha) \quad (4.3)$$

where α denotes liquid water or ice phase, and 0 superscript/subscripts stands for reference condition. Δh_w and Δv_w are enthalpy change and volume difference between the empty hydrate lattice and water in α phase, respectively. The parameters for Eqs. (4.2) and (4.3) are provided in Tables 4.1 and 4.2.

The impact of any additives in the mixture can be seen on three parameters of Eqs. (4.2) and (4.3), i.e. fugacity, activity of water, and Langmuir constant. The first parameter is fugacity of components in Eq. (4.2). Addition of any extra component in the mixture will change the phase equilibria, and consequently the fugacity of each component in the mixture. In the calculation of fugacity in the vdWP model, it commonly assumed that at equilibrium, the amount of hydrate particles is very small, and the system mainly consisted of two phases of vapour and liquid/solid water. Therefore, any VLE or VSE calculation with proper mixing rule could lead to an acceptable prediction of fugacity. Thus, the most critical task in the calculation of fugacity is a selection of suitable equation of state and mixing rule. While EOSs such as Peng–Robinson [12] or Soave–Redlich–Kwang [13] with van der Waals mixing

Table 4.1 Geometry of different hydrate structures and parameters used in Eqs. (4.2), (4.5), and (4.6)

Hydrate structure	Structure I		Structure II		Structure H		
	Small	Large	Small	Large	Small	Medium	Large
Cavity name	5 ¹²	5 ¹² 6 ²	5 ¹²	5 ¹² 6 ⁴	5 ¹²	4 ³ 5 ⁶ 6 ³	5 ¹² 6 ⁸
Average radius (R) (Å)	3.91	4.33	3.9	4.68	3.94	4.04	5.79
Coordination number (z)	20	24	20	28	20	20	36
Cavities/unit cell	2	6	16	8	3	2	1
Cavities/H ₂ O (v_m)	1/23	3/23	2/17	1/17	1/12	1/18	1/36
H ₂ O/unit cell	46		136		36		
Crystal type	Cubic		Cubic		Hexagonal		
Lattice constant (m)	1.20 × 10 ⁻¹¹		1.72 × 10 ⁻¹¹		$a = 1.22 \times 10^{-11}$ $c = 1.01 \times 10^{-11}$		

Table 4.2 Thermodynamic properties of the empty hydrate lattice relative to liquid water, Eq. (4.3)

Parameter	Structure sI	Structure sII
$\Delta\mu_w^o$ (J/mol)	1263.6	882.8
Δh_w^o (J/mol)	-4858.9	-5202.2
Δv_w^l (cm ³ /mol)	4.6	5.0
ΔC_{Pw} (J/mol K)	-38.12 + 0.141($T - 273.15$)	

rule can be used for hydrocarbon systems, for more complex systems, including electrolytes or very polar components, a more advanced equation of state, such as Valderrama–Patel–Teja [14], Nasrifar–Bolland [15], CPA [16], or statistical associating fluid theory (SAFT) equations of state [17], leads to better prediction. Moreover, the G-excess mixing rules such as MHV1 [18] or MHV2 [19] would increase the accuracy of fugacity calculations.

The second parameter is the activity of water, which is presented in Eq. (4.3). The water activity will change significantly in the presence of additives, especially thermodynamic hydrate inhibitors. Therefore, to predict the impact of these additives on the hydrate equilibria, it is important to calculate the water activity quite accurate. This is not an easy task, as hydrate equilibrium involves multicomponents system at high-pressure and low-temperature conditions and most of activity models are designed for low pressures and binary systems. However, combining VLE calculation with G-excess mixing rules and exploitation of a predictive activity model such as UNIFAC or UNIQUAC could lead to reasonable accuracy in calculation of water activity in the liquid phase.

The third parameter, which is the Langmuir constant, is more important for systems containing thermodynamic promoters. While the majority of thermodynamic inhibitors are not involving in the crystalline structure of gas hydrate, some of the promoters either work as hydrate formers (e.g. tetrahydrofuran, acetone, 1-4 dioxane [20]) or as part of crystalline building blocks (e.g. tetra-n-butyl ammonium bromide [21]). While prediction of hydrate formation condition in the presence of second group is needed more complicated modelling, the first group, i.e. that work as hydrate formers, can be predicted by considering as a hydrate former. This includes calculating fugacity, activity, and Langmuir constant for these chemicals.

To calculate the Langmuir constant, two methods are generally used in literature. The first and easier method was developed by Parrish and Prausnitz [9] which is a correlation suitable for the temperature range of 260–300 K, as shown in Eq. (4.4)

$$C_{m,i}(T) = (A_{m,i}/T) \exp(B_{m,i}/T) \quad (4.4)$$

The values for $A_{m,i}$ and $B_{m,i}$ parameters are given for each hydrate former i that filled cavity type m in either structure sI or sII by Parrish and Prausnitz [9] and presented in Table 4.3.

The more accepted method is based on the intermolecular interaction between hydrate former and water molecules in a hydrate cavity, Van der Waals and Platteeuw by using Lennard–Jones–Devonshire cell theory to calculate the Langmuir constant, as shown in Eq. (4.5).

$$C_{m,i}(T) = 4 \frac{\pi}{kT} \int_0^{R_m - 2a_i} \exp\left[-\frac{\omega_{m,i}(r)}{kT}\right] r^2 dr \quad (4.5)$$

Table 4.3 Parameters for calculating Langmuir constants by Eq. (4.4) between 260 and 300 K

Guest	Structure I				Structure II			
	Small (K)		Large (K)		Small (K)		Large (K)	
	$A_{m,i} \times 10^3$	$B_{m,i} \times 10^{-3}$	$A_{m,i} \times 10^3$	$B_{m,i} \times 10^{-3}$	$A_{m,i} \times 10^3$	$B_{m,i} \times 10^{-3}$	$A_{m,i} \times 10^3$	$B_{m,i} \times 10^{-3}$
Nitrogen	3.8087	2.2055	18.42	2.3013	3.0284	2.175	75.149	1.8606
Carbon dioxide	1.1978	2.8605	8.507	3.2779	0.9091	2.6954	48.262	2.5718
Methane	3.7237	2.7088	18.372	2.7379	2.956	2.6951	76.068	2.2027
Ethane	0	0	6.906	3.6316	0	0	40.818	3.0384
Propane	0	0	0	0	0	0	12.353	4.4061
Isobutane	0	0	0	0	0	0	1.573	4.453
Ethylene	0.083	2.3969	5.448	3.66638	0.0641	2.0425	34.94	3.1071
Propylene	0	0	0	0	0	0	20.174	4.0057
Hydrogen sulphide	3.0343	3.736	16.74	3.6109	2.3758	3.7506	73.631	2.8541

where k is the Boltzmann constant, $\omega(r)$ is the spherically symmetric cell potential that is a function of cell radius, r , and T is the absolute temperature. R_m is the type m cavity radius and a_i is the hydrate former i core radius. Parrish and Prausnitz recommend the Kihara theory for calculation of cell potential, as shown in Eq. (4.6).

$$\omega_{m,i}(r) = 2z_m \varepsilon_i \left[\frac{\sigma_i^{12}}{R_m^{11} r} \left(\delta^{10} + \frac{a_i}{R_m} \delta^{11} \right) - \frac{\sigma_i^6}{R_m^5 r} \left(\delta^4 + \frac{a_i}{R_m} \delta^5 \right) \right] \quad (4.6)$$

where ε_i is the minimum potential, $\sigma_i + 2 a_i$ is the collision diameter, z_m is the coordination number of each cavity, and δ^N is calculating with Eq. (4.7) for N equals to 4, 5, 10, and 11.

$$\delta^N = \frac{\left[\left(1 - \frac{r}{R_m} - \frac{a_i}{R_m} \right)^{-N} - \left(1 + \frac{r}{R_m} - \frac{a_i}{R_m} \right)^{-N} \right]}{N} \quad (4.7)$$

ε_i , σ_i , and a_i are the Kihara potential parameters that are optimized with hydrate equilibrium data and given for each hydrate former. The values for common hydrate formers are given in Table 4.4. The z_m and R_m values also given in Table 4.1.

Table 4.4 Kihara parameters of common hydrate formers and thermodynamic promoters [22]

Component	a (Å)	σ (Å)	$\bar{\epsilon}/k$ (K)
Nitrogen	0.3526	3.0124	125.15
Carbon dioxide ^a	0.6358	2.9681	169.09
Methane	0.3834	3.1650	154.54
Ethane	0.5651	3.2641	176.40
Propane	0.6502	3.3093	203.31
Isobutane	0.8706	3.0822	225.16
Ethylene	0.4700	3.2910	172.87
Propylene	0.6500	3.2304	202.42
Hydrogen sulphide	0.3600	3.1530	204.85
THF ^a	0.8830	3.0020	301.95
Acetone ^a	0.96785	2.9297	283.62

^aOptimized values [23]

4.3 Suppression Temperature Models

As mentioned before, the hydrate equilibrium temperature gradually reduces in the presence of inhibitors due to the intermolecular interaction between these chemicals and water molecules. From a thermodynamic point of view, these interactions reduce the water molecule's activity. Pieroen [24] formulated a relationship between enthalpy of hydrate formation, water activity, and suppression temperature, as shown in Eq. (4.8).

$$\ln(a_w) = \frac{-\Delta H^d}{n_H R} \left(\frac{1}{T} - \frac{1}{T_w} \right) \quad (4.8)$$

In this equation, a_w is the water activity in the presence of additives, n_H is the hydration number and ΔH^d is the enthalpy of hydrate dissociation, and T and T_w are the hydrate equilibrium temperature in the presence of additives and pure water, respectively. Since the values of a_w , n_H , and ΔH^d cannot be easily calculated, Pieroen showed that by a good approximation, this equation could be simplified to calculate the suppression temperature, as shown in Eq. (4.9).

$$\Delta T = -\frac{n_H R T_0^2}{\Delta H^d} \frac{18W}{M(100 - W)} \quad (4.9)$$

Equation (4.9) is very similar to Eq. (4.1) that was developed by Hammerschmidt based on the experimental data. Later, Maddox et al. [25] used the Pieroen formula to calculate the hydrate equilibrium temperature in the presence of alcohols. They suggested using Margules's equation for calculating the activity coefficient of water, as shown in Eq. (4.10). Additionally, they developed a model to calculate $\Delta H^d/n_H R$, as presented in Eq. (4.11).

$$\ln(\gamma_w) = (1 - x_w)^2[B + 2x_w(A - B)] \quad (4.10)$$

$$\frac{\Delta H^d}{n_H R} = \frac{-2063}{\alpha + \frac{\beta P}{1000} + \delta \ln P} \quad (4.11)$$

In these equations, A and B are the Margules constant for each electrolyte or alcohol, x_w is the mole fraction of water in the solution, and α , β , and δ are the coefficients that encounter the pressure dependency of enthalpy of hydrate dissociation. Later, Javanmardi et al. [26] modified the enthalpy equation and included the ionic strength of solution in order to use this method for electrolytes system.

$$\frac{\Delta H^d}{n_H R} = \frac{e_1 I^{e_2}}{1 + e_3 P + e_4 \ln P} \quad (4.12)$$

In this equation, I is ionic strength and e_1 to e_4 are global constants. Javanmardi and his co-workers [26, 27] calculated the coefficients' value by fitting the equilibrium data of different gas hydrate system in the presence of various electrolytes. Later, Nasrifar et al. [28] optimized the parameters of Eq. (4.12) by increasing the database. Partoon et al. [29] also extended the model to ionic liquid systems. However, they provided another set of parameters for ionic liquids. The coefficients of Eq. (4.12) are presented in Table 4.5.

Javanmardi et al. suggested to use more complicated model of Pitzer and Mayorga [30], as shown in Eqs. (4.13)–(4.17).

$$\ln a_w = \frac{-vmM_w}{\varphi} \quad (4.13)$$

$$-1 = |z^+ z^-| f^\varphi + m \left(\frac{2v^+ v^-}{v} \right) \beta_{MX}^\varphi + m^2 \left(\frac{2(v^+ v^-)^{\frac{3}{2}}}{v} \right) C^\varphi \quad (4.14)$$

$$f^\varphi = -A_\varphi \frac{I^{\frac{1}{2}}}{1 + bI^{\frac{1}{2}}} \quad (4.15)$$

$$\beta_{MX}^\varphi = \beta^{(0)} + \beta^{(1)} \exp(-aI^{\frac{1}{2}}) \quad (4.16)$$

Table 4.5 Parameters of Eq. (4.12)

Parameter	Electrolytes [26]	Electrolytes [28]	Ionic liquids [29]
e_1	597.33	1000.0	222.24
e_2	-4.090×10^{-2}	1.237×10^{-2}	-7.796×10^{-2}
e_3	2.270×10^{-5}	-1.205×10^{-2}	3.854×10^{-5}
e_4	-7.510×10^{-2}	4.073×10^{-2}	2.530×10^{-2}

$$I = 0.5 \sum m_i z_i^2 \quad (4.17)$$

In these equations, φ is the osmotic coefficient, M_w is water molecular weight, ν^+ and ν^- are number of ions in the salt formula, and z^+ and z^- are number of cation and anion charges, respectively. Also, $\nu = \nu^+ + \nu^-$, m is the conventional molality of each ion (anion and cation) and z_i is the number of each cation and anion charges. As suggested by Pitzer and Mayorga, $a = 2$ and $b = 1.2$ for all electrolytes. $\beta^{(0)}$, $\beta(1)$ and C^φ are model parameters that are available for each electrolyte. The parameter A_φ is the Debye–Hückel coefficient. Javanmardi et al. [26] used a value of 0.392 for water at 25 °C in their study; however, A_φ is a weak function of temperature. Therefore, Partoon et al. [29] suggested to use the temperature-dependent Debye–Hückel coefficient, as presented in Eq. (4.18) [31], for calculating the activity coefficient.

$$A_\varphi = 0.3769 + 0.0005(T - 273.15) + 0.000004(T - 273.15)^2 \quad (4.18)$$

The described method, however, is limited to a single additive. For a mixture of electrolytes, Nasrifar et al. [28] suggested to use Patwarthan and Kumar's [32] mixing rule for activity coefficient, as shown in Eq. (4.19).

$$\ln a_w = \sum_k (m_k/m_k^0) \ln a_{w,k}^0 \quad (4.19)$$

In addition, Nasrifar et al. [28] suggested another mixing rule for a mixture containing both electrolytes and alcohols, as it is the most probable case for real application of inhibitors in the oil and gas transportation pipelines. First, for calculating the water activity, Nasrifar et al. [28] suggested that the non-idealistic reasoning to suppress water in the presence of electrolytes and alcohols are independent. Therefore, the total non-idealistic factor is cumulative, as shown in Eq. (4.20).

$$\ln a_{w,\text{mix}} = \ln a_{w,\text{el}} + \ln a_{w,\text{al}} \quad (4.20)$$

where $a_{w,\text{mix}}$ the is calculated be Eq. (4.14) and $a_{w,\text{al}}$ is calculated by Eq. (4.10). In addition, the enthalpy of hydrate dissociation for the mixture of electrolytes and alcohols are calculated by Eq. (4.21).

$$\left(\frac{\Delta H^d}{n_H R}\right)_{\text{mix}} = \frac{2\left(\frac{\Delta H^d}{n_H R}\right)_{\text{el}}\left(\frac{\Delta H^d}{n_H R}\right)_{\text{al}}}{\left(\frac{\Delta H^d}{n_H R}\right)_{\text{el}} + \left(\frac{\Delta H^d}{n_H R}\right)_{\text{al}}} \quad (4.21)$$

where $\left(\frac{\Delta H^d}{n_H R}\right)_{\text{al}}$ and $\left(\frac{\Delta H^d}{n_H R}\right)_{\text{el}}$ are calculated by Eqs. (4.11) and (4.12), respectively.

Another approach for the calculation of hydrate suppression temperature was developed by Dickens and Quinby-Hunt [33]. The model considered the Pieroen

equation (Eq. 4.8) as the base for calculation for the suppression temperature. However, as the calculation of the activity coefficient was complicated, they suggested to use the freezing point suppression temperature instead of activity coefficient, as shown in Eq. (4.22).

$$\ln a_w = \frac{\Delta H_{\text{Fus}}}{R} \left(\frac{1}{T_f^0} - \frac{1}{T_f} \right) \quad (4.22)$$

where ΔH_{Fus} is the enthalpy of fusion of pure water, T_f^0 is the ice point and is the suppressed melting point of solution. Combining Eqs. (4.8) and (4.22), the activity of water in the presence of additives is eliminating from the formula, as presented in Eq. (4.23), resulting in simpler method for prediction of hydrate suppression temperatures.

$$\left(\frac{1}{T_w} - \frac{1}{T} \right) = \frac{n_h \Delta H_{\text{Fus}}}{\Delta H^d} \left(\frac{1}{T_f^0} - \frac{1}{T_f} \right) \quad (4.23)$$

However, as the activity calculations are well developed for electrolytes and alcohols, other researchers have not practiced the model. Nonetheless, recently, Bavoh et al. [34] and later Khan et al. [35] showed the potential of this model for calculation of the hydrate suppression temperature in the presence of natural amino acids and ionic liquid, where the activity coefficient cannot be estimated due to the presence of electrolytes and alcohols.

The Pieroen formula was also used to predict the hydrate equilibrium temperature in the presence of acetone by Mainusch et al. [36]. The major modification in this model was in the calculation of $\Delta H^d / n_H R$, as shown in Eq. (4.24).

$$\begin{aligned} & \frac{\Delta H^d}{n_H R} \\ &= \frac{-31.3 - (3.0 \times 10^3)x_a - (3.7 \times 10^5)x_a^{4.5} + (3.36 \times 10^8)x_a^{13.5}}{1 - (9.3 \times 10^{-2}) \ln(P/P^0)} \end{aligned} \quad (4.24)$$

where x_a is the mole fraction of acetone in the mixture and P is the system pressure. The P^0 is the reference pressure and is equal to 1 kPa. The activity coefficient of water in the presence of acetone was calculated using the van Laar equation [36]. However, this formula can only be used for CH_4 hydrates, where the acetone acts as promoter, while, for other gases like CO_2 , it can act as inhibitor. Partoon [23] modified the Pieroen formula to adapt it for other hydrate thermodynamic promoters, i.e. water soluble hydrate hydrocarbons, by introducing the polarity index ratio in the calculation as shown in Eq. (4.25) and (4.26).

$$\ln(a_w) = \frac{-\Delta H^d}{n_H R} \text{PIC} \left(\frac{1}{T} - \frac{1}{T_w} \right) \quad (4.25)$$

$$\text{PIC} = 10 \left(\sum_{i=1}^{nc} j_i \cdot \text{PIR} \cdot \ln \left[\frac{1 - x_i}{\sum_{\substack{j=1 \\ j \neq w}}^{nc} x_j} \right] \right) \quad (4.26)$$

$$\text{PIR} = \ln \left(\frac{2\text{PI}_i + 1}{\text{PI}_w} \right) \quad (4.27)$$

where PI_i is the polarity index of solvent and PI_w is the polarity index of water which is equal to 10.2 [37]. x_i is the mole fraction of gases in the pure water at hydrate equilibrium temperature and pressure. j_i is an index number that shows the impact of solvent on the pure gas hydrate. The value of j_i is equal to +1 if the impact of solvent on pure gas i hydrate is promotion and is equal to -1 if the solvent acts as inhibitor for gas i hydrate. Finally, the enthalpy of the hydrate disassociation is calculated using Eq. (4.28).

$$\frac{\Delta H^d}{n_H R} = \frac{-56.7 + ax_a + bx_a^{\text{PI}} + cx_a^{2\text{PI}}}{1 + d \ln(P/P^\circ)} \quad (4.28)$$

4.4 Kinetic Models for Growth of Gas Hydrates

The growth of gas hydrates usually takes place after nucleation and is a complex phenomenon as it includes multiphase studies at various levels of research. On a macroscopic scale, the kinetics of gas hydrate growth usually depends on the mole consumption rate of gases. At the microscopic level, the growth of gas hydrates can be quantified as:

1. Mass transfer of H_2O and gases for the growth of hydrate surface.
2. Transportation of exothermic heat produced during crystal growth of gas hydrates.
3. The intrinsic kinetics of gas hydrates growth.

Based on all these factors, the structure of gas hydrates has been classified.

A substantial amount of literature has been published (Table 4.6) in which all major gas hydrate growth models on kinetics are displayed since 1980. Most of these models that are mentioned here are not developed from the principles, and most of them cover the multiphase patterns. Moreover, there is no uniform model, which covers all the significant aspects of kinetics of growth of gas hydrates. So, still, there is a significant research contribution that needs to be made in this area.

Table 4.6 Summary of kinetic growth models

Controlling mechanism	Model features/driving force/rate equation	References	Chemical combination
Reaction kinetics	<p>Arrhenius-type rate equation $r = Aa_s \exp\left(-\frac{\Delta E_a}{RT}\right) \exp\left(-\frac{a}{\Delta T^b}\right) P^\gamma$</p> <p>The reaction rate law for first order (mole fraction)</p> $r = K_R * x_G(t)$ <p>Pseudo-reactions that are elementary and included with rate constants</p> <p>Arrhenius-type rate equation with sub cooling as the driving force</p> $r = uk_1 \exp\left(-\frac{k_2}{RT}\right) A_s (T_{eq} - T_{sys})$	<p>[38, 39]</p> <p>[40]</p> <p>[41–43]</p>	<p>CH₄ + Glycol</p> <p>C₂H₆ + Glycol</p> <p>CO₂ + Ethylene Glycol</p> <p>CH₄ + Methanol</p>
Mass transfer	<p>Model due to concentration difference between phases of gas and liquid</p> <p>Fugacity difference if gas phase with population balance model</p> $r = \sum_j^2 K_j^* A_p (f - f_{eq,j})$ <p>Concentration difference of CH₄ between the oil phase and equilibrium</p> $r = k_{g-0} A_{g-0} (C_{CH_4,0}^{eq} - C_{CH_4,0})$ <p>Model due to concentration difference (advanced nucleation)</p> $r = k_g (C_b - C_{eq})$	<p>[44, 45]</p> <p>[46]</p> <p>[47]</p> <p>[48, 49]</p>	<p>CH₄, C₂H₆</p> <p>CH₄ + Glycol</p> <p>C₂H₆ + Glycol</p> <p>CO₂ + Glycol</p> <p>CH₄ + Methanol</p> <p>CH₄ + Glycol</p>
Heat transfer	<p>1D H.T model due to conduction</p> <p>1D H.T model due to conduction and convection</p> $\nu r \delta = \Delta T^{3/2}$ <p>1D H.T model due to convection</p> $\nu r \delta = \psi \Delta T^{5/2}$ <p>2D H.T model due to conduction</p>	<p>[50–53]</p>	<p>CO₂</p> <p>CO₂</p> <p>CH₄, C₂H₄, CH₄ + C₂H₄</p> <p>CO₂</p>

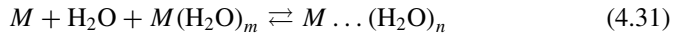
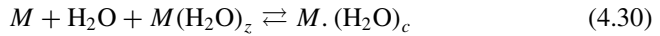
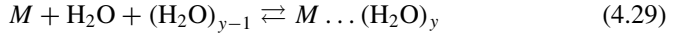
(continued)

Table 4.6 (continued)

Controlling mechanism	Model features/driving force/rate equation	References	Chemical combination
Models based on kinetic reactions and mass transfer	<p>Concentration difference with mass transfer and reaction kinetics</p> $r = K(C_{\text{sol}} - C_{\text{eq}})$ $\frac{1}{\bar{k}} = \frac{1}{k_L A_g} + \frac{1}{k_s A_c}$ <p>Mass transfer at liquid-vapour interface and reaction kinetics</p> $r = \frac{1}{A_p} \left(\frac{1}{k_{H-L}} + \frac{1}{\bar{k}_r} \right) + \frac{1}{k_{G-L}}$ <p>Shrinking core model with diffusion or reaction coupled</p> $(1 - \alpha)^{1/3} = \left(-\frac{(2k)^{1/2}}{r_0} \right) (t - t^*)^{1/2} + (1 - \alpha^*)^{1/3}$ <p>Molecular diffusion with first-order formation kinetics of water</p> <p>Molecular diffusion with first-order formation and dissociation kinetics of H₂O</p> <p>Molecular diffusion with first-order formation kinetics of CO₂</p> <p>Reaction-limited and diffusion-limited schemes with induction time</p>	<p>[54]</p> <p>[55]</p> <p>[56–58]</p> <p>[59–62]</p> <p>[63]</p> <p>[64]</p>	<p>CH₄ + Methanol</p> <p>C₃H₈ + MEG</p> <p>CH₄ + H₂O</p> <p>CH₄ + D₂O</p> <p>CO₂</p> <p>CO₂(LCO₂),</p> <p>CO₂</p> <p>CO₂</p> <p>CH₄ + CaCl₂</p>
Models based on kinetic reactions and heat transfer	<p>Kinetic rate joined with H.T. model</p> $\frac{dX}{dt} = \frac{\Delta T}{\rho_h \lambda \left(\frac{1}{k \Delta T^m} + \frac{1}{h_{\text{avg}}(T)} \right)}$ <p>Surface kinetic rate joined with H.T. model</p> $\frac{dX}{dt} = \frac{T_{\text{eq}} - T_{\text{bulk}}}{\Delta T} \frac{1}{\frac{k_p A_h}{k_p A_h} + k_r A_r}$ <p>Kinetic rate joined with a heat convection model</p> $\frac{dX}{dt} = \frac{T_{\text{eq}} - T_{\text{bulk}}}{\rho_h \lambda \left(\frac{1}{k} + \frac{1}{h} \right)}$ <p>Equilibrium model in sandy porous medium</p>	<p>[65]</p> <p>[66]</p> <p>[67]</p> <p>[68–71]</p>	<p>Tetrahydrofuran</p> <p>CH₄, CO₂</p> <p>CH₄ + Diesel Oil</p> <p>CH₄</p>
Fluid flow heat flow and reaction kinetics	<p>Kinetic rate equation of hydrate formation and hydrate dissociation</p> <p>Kinetic rate equation based on the model of Kim et al.</p> <p>Simple slug flow model joined with kinetic rate and heat flow</p>	<p>[72]</p> <p>[73]</p>	<p>CH₄, CO₂</p> <p>CH₄</p> <p>CH₄</p>

4.4.1 Models Based on Chemical Reaction

Experiments were conducted for investigation of the kinetics of growth rate of gas hydrates of methane and ethane, and a two-step procedure is described which starts with the formation of the crystal due to the interface between gas and water molecules. The following is the three-step rate equations that are considered as the Arrhenius equations:



By a combination of these equations, the rate of hydrate formation is termed as follows:

$$r = k_r a_s [\text{H}_2\text{O}]^m [\text{H}_2\text{O}]_c^n [M]^q \quad (4.32)$$

where

k_r	constant of reaction rate for lumped Arrhenius type
a_s	total surface area of the gas–water interface
$m, n, \text{ and } q$	parameters indicating the order of reaction for each component
c	critical cluster size.

This kinetic model is adopted by many researchers in later years to study the rate of growth of gas hydrates. These studies included bubble theory in deep sea conditions that affect gas hydrate formation. This bubble theory was further used to analyse blow-out conditions of oil wells in the presence of water. Later, this model is further improved by the addition of heat and mass balance equations alongside considering the drag effect of a slug on the multiphase flow. Later around 1993, research interest was concentrated on liquid water approach with CH_4 gas to analyse the kinetics of gas hydrate growth. A critical model was proposed with five elemental processes considering three-step analysis of hydrate formation:

1. The dissolution of CH_4 gas into H_2O phase
2. The build-up of CH_4 hydrate precursor
3. The growth of CH_4 hydrate by an autocatalytic process.

This model was also accounted for in the development of a kinetic model for analysis of gas hydrate formation in oil-dominated systems. These intrinsic models are used and impended into commercial software like CSMhyk for analysis of different hydrate formation kinetics.

The concentration shifted slowly from CH_4 to CO_2 with the time. The study of carbon dioxide hydrates came into importance and studies mentioned that the hydrate

growth is dependent on interfacial temperatures and pressures of phases. Experimental results were claimed that the multiphase flow regimes affect the rate of formation of gas hydrates. Also, studies presented displayed that the kinetic models based on heat transfer and mass transfer are not much different when it comes to results of the kinetics of growth rate of gas hydrates. However, some of the models are unclear, and many errors were still included in the model due to the difficulty in predicting the accuracy of gas–liquid interphase. Moreover, the models developed based on experimental results have a limitation as many of them are apparatus dependent. They might not be applicable to real-time systems as their capacity is higher compared to laboratory scale equipment. Later, an advanced model proposed by Lekvam et al. states that the rate of reaction can be estimated and validated by means of vital statistics. This helps as a significant model that reduces the research gap between the microscopic and macroscopic level of study on the kinetics of gas hydrates. It also can be displayed as the proof for the representation of “chemical reaction” for the formation of gas hydrates.

4.4.2 Models Based on Mass Transfer

The reported kinetic model was proposed in 1987 with referring to the methane and ethane gas hydrates. The major part of their study was reported because of the fugacity differences dissolved gas and multiphase hydrate equilibrium at a constant temperature T . The model was developed based on the theory of the growth of crystallization of gas hydrates. Surprisingly, this model gave a very less dependence on T , unlike chemical reaction models. According to the proposed model, the following two consecutive steps of hydrate particle growth were proposed:

- Diffusion of the dissolved gas from the bulk of solution to the crystal–liquid interface
- Adsorption process that incorporates the gas molecules into the water molecules and the subsequent stabilization of the framework of the structured water.

An assumption is made in this model about the shape of the hydrate particles which are spherical and uniformly distributed. The fugacity changed from initial stages to final stages in diffusion and adsorption layers, and the difference between initial and final conditions can be termed as an overall driving force. The rate of growth of hydrate particles can be found by:

$$\frac{dn}{dt} = K^* A_p (f_b - f_{eq}) \quad (4.33)$$

$$\frac{1}{K^*} = \frac{1}{K_r} + \frac{1}{K_d} \quad (4.34)$$

where

- A_p surface area of hydrate particle
 K^* overall kinetic rate constant
 K_r Rate of reaction due to adsorption
 K_d mass transfer rate.

The overall rate of reaction for all included particles can be found by integrating each particle of all sizes. It can be found by

$$R_y(t) = \int_0^{\infty} \left(\frac{dn}{dt} \right) \varnothing(r, t) dr = 4\pi K^* \mu_2 (f - f_{eq}) \quad (4.35)$$

$$\mu_2 = \int_0^{\infty} r^2 \varnothing(r, t) dr \quad (4.36)$$

where \varnothing is the particle size of hydrate and μ_2 is the second moment of the particle size.

When the gas phase encounters liquid phase, two-film theory was adopted. In this theory, quasi-steady-state condition is considered. Thus, the diffusion rate of gas from the interface of gas-liquid was balanced. The mass balance of gas molecules is given by:

$$D \frac{d^2 C}{dy^2} = 4\pi K^* \mu_2(t) (f - f_{eq}) \quad (4.37)$$

B.C. 1: $C_{(0)} = C_{eq}$

B.C. 2: $C_{(\delta)} = C_b$

where “ δ ” = liquid film thickness.

After adopting Henry’s law of fugacity to develop a profile of fugacity of the gas, the flux of gas that is being transported can be derived by

$$f_{(y)} = f_{eq} + \left(\frac{1}{\sin h \gamma} \right) \left\{ (f_g - f_{eq}) \sin h \left(\gamma \left(1 - \frac{y}{\delta} \right) \right) + (f_b - f_{eq}) \sin h \left(\gamma \frac{y}{\delta} \right) \right\} \quad (4.38)$$

$$\frac{dn}{dt} = J_{y=0} A_{g-1} = \left(\frac{D^* \gamma A_{g-1}}{\delta} \right) \frac{((f_g - f_{eq}) \cos h \gamma - (f_b - f_{eq}))}{\sin h \gamma} \quad (4.39)$$

$$\gamma = \delta \sqrt{\frac{4\pi K^* \mu_2}{D^*}} \quad (4.40)$$

$$D^* = \frac{DC_{wo}}{H} \quad (4.41)$$

where

- γ Hatta number
- H Henry's law constant
- D diffusion coefficient
- C_{wo} initial water concentration
- f_g fugacity of pure gas
- f_b gas fugacity of liquid bulk.

Alongside these advanced studies, many more studies on the kinetics of gas hydrates have been done. Some of them are kinetic models that are developed using concentration difference between gases, models that are based on the combination of mass and heat transfer due to chemical reactions of gas and fuels during hydrate formation. Some studies also covered the kinetics of gas hydrates in porous media.

So, as discussed in this chapter from the past 30 years, considerable progress has been made regarding the study of the kinetics of gas hydrate growth. In brief, this chapter covered most of the significant kinetic models that involve various combinations regarding the growth of gas hydrates. This will serve as a reference for the development of advanced models in future. Interestingly, among all the models discussed, none of them covered both physical behaviours of the formation of gas hydrates. So, still, there is a need for the united kinetic growth model proposal. This unified model should cover all the physical parameters that influence the kinetics of gas hydrates. Even though many models that are developed are used industrially, still there is a lack of accuracy when scaling them upon more extensive apparatus. So, by the study done here, a next-generation model can be made to bridge the gap between the applications of the developed models on an industrial perspective.

References

1. Hammerschmidt EG (1934) Formation of gas hydrates in natural gas transmission lines. *Ind Eng Chem* 26:851–855
2. Campbell JM (1992) Gas conditioning and processing-volume 2: the equipment modules. *Campbell Petroleum Series*.
3. Sloan ED, Koh CA (2008) *Clathrate hydrates of natural gases* third edition. CRC Press, Boca Raton, p 119
4. Carroll JJ (2009) *Natural gas hydrates: a guide for engineers*, 2nd edn. Gulf Professional Publishing, Burlington
5. Dyadin YA, Zhurko FV, Bondaryuk IV, Zhurko GO (1991) Clathrate formation in water-cyclic ether systems at high pressures. *J Incl Phenom Mol Recogn Chem* 10(1):39–56
6. Barrer RM, Stuart WI (1957) Non-stoichiometric clathrate compounds of water. *Proc R Soc Lond Ser A. Math Phys Sci* 243(1233):172–189
7. Waals JVD, Platteeuw JC (1958) Clathrate solutions. *Adv Chem Phys* 1–57
8. Saito S, Marshall DR, Kobayashi R (1964) Hydrates at high pressures: Part II. Application of statistical mechanics to the study of the hydrates of methane, argon, and nitrogen. *AIChE J* 10(5):734–740
9. Parrish WR, Prausnitz JM (1972) Dissociation pressures of gas hydrates formed by gas mixtures. *Ind Eng Chem Process Des Dev* 11:26–35

10. Holder GD, Corbin G, Papadopoulos KD (1980) Thermodynamic and molecular properties of gas hydrates from mixtures containing methane, argon, and krypton. *Ind Eng Chem Fundam* 19:282–286
11. John VT, Papadopoulos KD, Holder GD (1985) A generalized model for predicting equilibrium conditions for gas hydrates. *AIChE J* 31:252–259
12. Peng DY, Robinson DB (1976) A new two-constant equation of state. *Ind Eng Chem Fundam* 15:59–64
13. Soave G (1972) Equilibrium constants from a modified Redlich-Kwong equation of state. *Chem Eng Sci* 27:1197–1203
14. Valderrama JO (1990) A generalized Patel-Teja equation of state for polar and nonpolar fluids and their mixtures. *J Chem Eng Jpn* 23:87–91
15. Nasrifar K, Bolland O (2006) Simplified hard-sphere and hard-sphere chain equations of state for engineering applications. *Chem Eng Commun* 193(10):1277–1293
16. Kontogeorgis GM, Voutsas EC, Yakoumis IV, Tassios DP (1996) An equation of state for associating fluids. *Ind Eng Chem Res* 35:4310–4318
17. Chapman WG, Gubbins KE, Jackson G, Radosz M (1989) SAFT: equation-of-state solution model for associating fluids. *Fluid Phase Equilibria* 52:31–38
18. Michelsen ML (1990) A modified Huron-Vidal mixing rule for cubic equations of state. *Fluid Phase Equilibria* 60:213–219
19. Dahl S, Michelsen ML (1990) High-pressure vapor-liquid equilibrium with a UNIFAC-based equation of state. *AIChE J* 36:1829–1836
20. Saito Y (1996) Methane storage in hydrate phase with water soluble guests. In: *Proceedings of 2nd international conference on natural gas hydrates, Toulouse, France, 2*, pp 459–465
21. Oyama H, Shimada W, Ebinuma T, Kamata Y, Takeya S, Uchida T, ... Narita H (2005) Phase diagram, latent heat, and specific heat of TBAB semiclathrate hydrate crystals. *Fluid Phase Equilibria* 234:131–135
22. Sloan Jr ED, Koh CA (2007) *Clathrate hydrates of natural gases*. CRC Press, Boca Raton
23. Partoon B (2017) Separation of carbon dioxide and methane via hydrate formation with utilization of modified spray reactor and thermodynamic promoters. Ph.D. Chemical Engineering Department, Universiti Teknologi PETRONAS, Perak, Malaysia
24. Pieroen AP (1955) Gas hydrates-approximate relations between heat of formation, composition and equilibrium temperature lowering by “inhibitors”. *Recl Des Trav Chim Des Pays-Bas* 74:995–1002
25. Maddox RN, Moshfeghian M, Lopez E, Tu CH, Shariat A, Flynn AJ (1991) Predicting hydrate temperature at high inhibitor concentration. In: *Proceedings of Laurance Reid gas conditioning conference, Norman, Oklahoma*, pp 273–294
26. Javanmardi J, Moshfeghian M, Maddox RN (1998) Simple method for predicting gas-hydrate-forming conditions in aqueous mixed-electrolyte solutions. *Energy Fuels* 12:219–222
27. Javanmardi J, Moshfeghian M, Maddox RN (1997) Simple method for predicting gas-hydrate-forming conditions in aqueous mixed-electrolyte solutions, 521–524
28. Nasrifar K, Moshfeghian M, Maddox RN (1998) Prediction of equilibrium conditions for gas hydrate formation in the mixtures of both electrolytes and alcohol. *Fluid Phase Equilibria* 146:1–13
29. Partoon B, Wong NM, Sabil KM, Nasrifar K, Ahmad MR (2013) A study on thermodynamics effect of [EMIM]-Cl and [OH-C2MIM]-Cl on methane hydrate equilibrium line. *Fluid Phase Equilibria* 337:26–31
30. Pitzer KS, Mayorga G (1993) Thermodynamics of electrolytes.: II. Activity and osmotic coefficients for strong electrolytes with one or both ions univalent. In: *Molecular structure and statistical thermodynamics: selected papers of Kenneth S Pitzer*, pp 396–404
31. Zemaitis Jr JF, Clark DM, Rafal M, Scrivner NC (2010) *Handbook of aqueous electrolyte thermodynamics: theory & application*. Wiley, New York
32. Patwardhan VS, Kumar A (1986) A unified approach for prediction of thermodynamic properties of aqueous mixed-electrolyte solutions. Part I: vapor pressure and heat of vaporization. *AIChE J* 32:1419–1428

33. Dickens GR, Quinby-Hunt MS (1997) Methane hydrate stability in pore water: a simple theoretical approach for geophysical applications. *J Geophys Res Solid Earth* 102:773–783
34. Bavoh CB, Partoon B, Lal B, Gonfa G, Khor SF, Sharif AM (2017) Inhibition effect of amino acids on carbon dioxide hydrate. *Chem Eng Sci* 171:331–339
35. Khan MS, Bavoh CB, Partoon B, Nashed O, Lal B, Mellon NB (2018) Impacts of ammonium based ionic liquids alkyl chain on thermodynamic hydrate inhibition for carbon dioxide rich binary gas. *J Mol Liq* 261:283–290
36. Mainusch S, Peters CJ, de Swaan Arons J, Javanmardi J, Moshfeghian M (1997) Experimental determination and modeling of methane hydrates in mixtures of acetone and water. *J Chem Eng Data* 42:948–950
37. Snyder LR (1974) Classification of the solvent properties of common liquids. *J Chromatogr A* 92:223–230
38. Sun C, Chen G, Guo T, Lin W, Chen J (2002) Kinetics of methane hydrate decomposition. *J Chem Ind Eng-China* 53:899–903
39. Vysniauskas A, Bishnoi PR (1985) Kinetics of ethane hydrate formation. *Chem Eng Sci* 40:299–303
40. Lekvam K, Ruoff P (1993) A reaction kinetic mechanism for methane hydrate formation in liquid water. *J Am chem Soc* 115:8565–8569
41. Boxall J, Davies S, Koh C, Sloan ED (2009) Predicting when and where hydrate plugs form in oil-dominated flowlines. *SPE Projects Facil Constr* 4:80–86
42. Zerpa LE, Sloan ED, Sum AK, Koh CA (2012) Overview of CSMHyK: a transient hydrate formation model. *J Pet Sci Eng* 98:122–129
43. Yang D, Le LA, Martinez RJ, Currier RP, Spencer DF (2011) Kinetics of CO₂ hydrate formation in a continuous flow reactor. *Chem Eng J* 172:144–157
44. Englezos P, Kalogerakis N, Dholabhai PD, Bishnoi PR (1987) Kinetics of gas hydrate formation from mixtures of methane and ethane. *Chem Eng Sci* 42:2659–2666
45. Englezos P, Kalogerakis N, Dholabhai PD, Bishnoi PR (1987) Kinetics of formation of methane and ethane gas hydrates. *Chem Eng Sci* 42:2647–2658
46. Skovborg P, Rasmussen P (1994) A mass transport limited model for the growth of methane and ethane gas hydrates. *Chem Eng Sci* 49:1131–1143
47. Herri JM, Pic JS, Gruy F, Cournil M (1999) Methane hydrate crystallization mechanism from in-situ particle sizing. *AIChE J* 45:590–602
48. Clarke MA, Bishnoi PR (2005) Determination of the intrinsic kinetics of CO₂ gas hydrate formation using in situ particle size analysis. *Chem Eng Sci* 60:695–709
49. Turner DJ, Miller KT, Sloan ED (2009) Methane hydrate formation and an inward growing shell model in water-in-oil dispersions. *Chem Eng Sci* 64:3996–4004
50. Uchida T, Ebinuma T, Kawabata JI, Narita H (1999) Microscopic observations of formation processes of clathrate-hydrate films at an interface between water and carbon dioxide. *J Crystal Growth* 204:348–356
51. Mori YH (2001) Estimating the thickness of hydrate films from their lateral growth rates: application of a simplified heat transfer model. *J Crystal Growth* 223(1–2):206–212
52. Peng BZ, Dandekar A, Sun CY, Luo H, Ma QL, Pang WX, Chen GJ (2007) Hydrate film growth on the surface of a gas bubble suspended in water. *J Phys Chem B* 111:12485–12493
53. Mochizuki T, Mori YH (2006) Clathrate-hydrate film growth along water/hydrate-former phase boundaries—numerical heat-transfer study. *J Crystal Growth* 290:642–652
54. Hashemi S, Macchi A, Servio P (2007) Gas hydrate growth model in a semibatch stirred tank reactor. *Ind Eng Chem Res* 46:5907–5912
55. Bergeron S, Servio P (2008) Reaction rate constant of propane hydrate formation. *Fluid Phase Equilibria* 265:30–36
56. Salamatin AN, Hondoh T, Uchida T, Lipenkov VY (1998) Post-nucleation conversion of an air bubble to clathrate air-hydrate crystal in ice. *J Crystal Growth* 193:197–218
57. Wang X, Schultz AJ, Halpern Y (2002) Kinetics of methane hydrate formation from polycrystalline deuterated ice. *J Phys Chem A* 106:7304–7309

58. Staykova DK, Kuhs WF, Salamatin AN, Hansen T (2003) Formation of porous gas hydrates from ice powders: diffraction experiments and multistage model. *J Phys Chem B* 107:10299–10311
59. Shindo Y, Lund PC, Fujioka Y, Komiyama H (1993) Kinetics of formation of CO₂ hydrate. *Energy Convers Manag* 34:1073–1079
60. Shindo Y et al (1993) Kinetics and mechanism of the formation of CO₂ hydrate. *Int J Chem Kinet* 25(9):777–782
61. Shindo Y, Sakaki K, Fujioka Y, Komiyama H (1996) Kinetics of the formation of CO₂ hydrate on the surface of liquid CO₂ droplet in water. *Energy Convers Manag* 37:485–489
62. Lund PC, Shindo Y, Fujioka Y, Komiyama H (1994) Study of the pseudo-steady-state kinetics of CO₂ hydrate formation and stability. *Int J Chem Kinet* 26:289–297
63. Dalmazzone D, Hamed N, Dalmazzone C (2009) DSC measurements and modelling of the kinetics of methane hydrate formation in water-in-oil emulsion. *Chem Eng Sci* 64(9):2020–2026
64. Teng H, Yamasaki A, Shindo Y (1996) Stability of the hydrate layer formed on the surface of a CO₂ droplet in high-pressure, low-temperature water. *Chem Eng Sci* 51:4979–4986
65. Freer EM, Selim MS, Sloan ED Jr (2001) Methane hydrate film growth kinetics. *Fluid Phase Equilib* 185:65–75
66. Mu L, Li S, Ma QL, Zhang K, Sun CY, Chen GJ, ... Yang LY (2014) Experimental and modeling investigation of kinetics of methane gas hydrate formation in water-in-oil emulsion. *Fluid Phase Equilib* 362:28–34
67. Rempel AW, Buffett BA (1997) Formation and accumulation of gas hydrate in porous media. *J Geophys Res Solid Earth* 102:10151–10164
68. Yin Z, Chong ZR, Tan HK, Linga P (2016) Review of gas hydrate dissociation kinetic models for energy recovery. *J Nat Gas Sci Eng* 35:1362–1387
69. Liu X, Flemings PB (2007) Dynamic multiphase flow model of hydrate formation in marine sediments. *J Geophys Res Solid Earth*, 112
70. Uddin M, Coombe D, Law D, Gunter B (2008) Numerical studies of gas hydrate formation and decomposition in a geological reservoir. *J Energy Resour Technol* 130:032501
71. Zerpa LE, Rao I, Aman ZM, Danielson TJ, Koh CA, Sloan ED, Sum AK (2013) Multiphase flow modeling of gas hydrates with a simple hydrodynamic slug flow model. *Chem Eng Sci* 99:298–304
72. Ribeiro CP Jr, Lage PL (2008) Modelling of hydrate formation kinetics: state-of-the-art and future directions. *Chem Eng Sci* 63:2007–2034
73. Yin Z, Khurana M, Tan HK, Linga P (2018) A review of gas hydrate growth kinetic models. *Chem Eng J* 342:9–29